Multicomponent lattice Boltzmann method for fluids with a density contrast

S. V. Lishchuk, I. Halliday, and C. M. Care
Materials and Engineering Research Institute, Sheffield Hallam University, Howard Street, Sheffield S1 1WB, United Kingdom
(Received 18 May 2007; revised manuscript received 5 September 2007; published 7 March 2008)

We present and verify a multicomponent lattice Boltzmann simulation scheme for two immiscible and incompressible fluids with a large density contrast. Our method is constructed from a continuum approximation description of a single inhomogeneous, and essentially incompressible, fluid. The equations that arise from this analysis are mapped onto an established multicomponent lattice Boltzmann method. The approach avoids the computational expense of a numerical solution of the fluid pressure field in a separate step. We present results obtained with our model which validate the initial assumptions and verify correct static and dynamic operation of the model up to a fluid density contrast ratio of more than 500. The paper concludes with an example that illustrates the potential utility of the approach by modeling a gas bubble rising under gravity and breaking through a free surface.

DOI: 10.1103/PhysRevE.77.036702 PACS number(s): 47.11.−j, 47.55.Ca

I. INTRODUCTION

Many multicomponent flows are concerned with two or more immiscible fluids which have a large relative density difference. This requirement has hampered the adoption of the otherwise promising multicomponent lattice Boltzmann method for the simulation of such situations. A number of authors have addressed this problem [1–6]. Inamuro *et al.* [1] report simulations with density contrasts of up to 1000. This is achieved by introducing a pressure correction derived from solutions of an appropriate Poisson equation. Similar density contrasts are achieved by (a) Lee and Lin [2] who use careful discretization of the lattice Boltzmann (LB) equations, (b) Wagner and Pooley [3] who reduce the speed of sound in a liquid-gas system, and (c) Zheng *et al.* [4] who employ an interface-capturing scheme based on the Cahn-Hilliard equation.

In this paper, we present an alternative LB scheme for modeling the flow of two immiscible and incompressible fluids that have a significant difference in density. The scheme is based upon a continuum description of a hypothetical, inhomogeneous fluid. It is computationally efficient and avoids, for example, the computational expense of solving for the fluid pressure field in an intermediate step as, for example, in [1].

The important distinction between existing large-density-difference LB methods [1,4] and the method reported here is the fact that our method is direct, easy to implement, and derives from continuum hydrodynamical principles alone; accordingly it may be seen as the most appropriate tool in large and very important classes of multicomponent flow calculations, which need to be made in the continuum regime.

Among the challenges encountered in continuum applications of multicomponent flow are the contrasting magnitudes of the interfacial tension parameter σ, the length and time scales, and the kinematic viscosity ν. The relative size of these parameters is, for our purposes, best expressed by the dimensionless Weber number

$$\mathrm{We} = 2\frac{\rho U^2 R}{\sigma}, \tag{1}$$

where R is the drop radius, ρ the density of the more dense fluid, and U the local velocity. In demonstrating our method, we shall attempt realistic, representative parametrizations, taking for our test bench example a breaching air bubble of a few centimeters diameter, rising under gravity, in water, characterized by $\mathrm{We}=O(1)$. In Sec. III C we consider in detail the parametrization of this problem; however, it should be stated at the outset that, to achieve so small a We, it was necessary, given our computational resources, to reduce to 10 the density contrast for our key results of Figs. 6 and 7 below: certainly other workers have achieved larger density contrasts with different LB schemes, but at much larger We, corresponding to much smaller surface tension parameters. Lee *et al.* and Mukherjee *et al.* achieve $\mathrm{We}=8000$ [2,6] and $\mathrm{We}\geq 20$ in [1]. Note also that, in the latter case, smaller We numbers were associated with increased spurious velocities, which are not a problem with the method presented here. Moreover, a density contrast of 10 is not particularly prohibitive, since the important physics of the problem (the momentum transfer from the less dense fluid) will not be significantly altered by using much larger density contrasts.

A. Overview of this paper

The key methodological elements of the technique presented here are presented as follows. (1) A single relaxation time LB model due to Qian *et al.* [7] is summarized in Sec. II A. (2) The surface tension between the two fluids is introduced using a scheme introduced in [8] and is explained in Sec. II B. (3) The phase separation of the fluids is achieved using a method based closely on the methods of d'Ortona *et al.* [9] and Latva-Kokko and Rothman [10] as set out in Sec. II C. (4) The method for introducing the effect of the large density difference through additional forcing at the interface is set out in Sec. III A. (5) The method of implementing the density difference scheme within a LB format is set out in Sec. III B. In order to achieve realistic parametrizations of the method, it is also found to be necessary to increase the stability of the LB scheme. This is achieved using a modification to the LB scheme due to Brownlee *et al.*[11]. Validating and illustrative results are given in Sec. IV and the conclusions are set out in Sec. V.

II. MULTICOMPONENT LATTICE BOLTZMANN METHOD

A. Single-component LB scheme

We use the single-relaxation-time, LB model due to Qian *et al.* [7]. The method is based upon the approximation of Bhathangar, Gross, and Krook (BGK) [12] for the Boltzmann collision operator and is hence commonly referred to as the *lattice BGK* (LBGK) method. A comprehensive review of LB methods is given, for example, by Succi [13].

The LB method is based upon an evolution equation for a discretized single-particle momentum distribution function f_i, to which a momentum source term $\phi_i(\mathbf{r})$ may be added:

$$f_i(\mathbf{r}+\delta_t\mathbf{c}_i,t+\delta_t)=f_i(\mathbf{r},t)+\omega[f_i^{(0)}(\rho,\rho\mathbf{u})-f_i(\mathbf{r},t)]+\phi_i(\mathbf{r}). \tag{2}$$

In the last equation, δ_t is the time step. The lattice on which this scheme is implemented has spacing δx. The term ϕ_i has the effect of impressing a force in the fluid by injecting momentum into the flow at each time step. The parameter ω lies in the range $0\leq\omega\leq 2$ and controls the fluid viscosity. It is shown below that the source term ϕ_i may be used to produce an interface between two immiscible fluids and also to introduce the effect of the difference in density between these two fluids.

The continuum hydrodynamic observables of density ρ and velocity $\mathbf{v}$ emerge from moments of the single-particle momentum distribution function f_i and an appropriately chosen equilibrium density $f_i^{(0)}(\rho,\rho\mathbf{v})$,

$$\rho(\mathbf{r},t)\equiv\sum_i f_i(\mathbf{r},t)=\sum_i f_i^{(0)}(\rho,\rho\mathbf{v}), \tag{3}$$

$$\mathbf{v}(\mathbf{r},t)\equiv\frac{1}{\rho}\sum_i f_i(\mathbf{r},t)\mathbf{c}_i=\frac{1}{\rho}\sum_i f_i^{(0)}(\rho,\rho\mathbf{v})\mathbf{c}_i. \tag{4}$$

In the presence of a constant source term ϕ_i, a Chapman-Enskog analysis [14] may be used to derive a weakly compressible form of the incompressible Navier-Stokes equations with a body force. In particular, the choice

$$\phi_i=t_p\frac{1}{k_2}\mathbf{F}\cdot\mathbf{c}_i \tag{5}$$

inserts a uniform pressure gradient $\mathbf{F}$ into the Navier-Stokes equations:

$$\rho\left(\frac{\partial}{\partial t}v_\alpha+v_\beta\frac{\partial}{\partial x_\beta}v_\alpha\right)=-\frac{\partial}{\partial x_\alpha}\delta p+\frac{\partial}{\partial x_\beta}(2\rho\nu S_{\alpha\beta})+F_\alpha. \tag{6}$$

Here we have used the summation convention on repeated subscripts, δp_0 represents a pressure fluctuation about a constant mean level, and

$$S_{\alpha\beta}=\frac{1}{2}\left(\frac{\partial v_\alpha}{\partial x_\beta}+\frac{\partial v_\beta}{\partial x_\alpha}\right) \tag{7}$$

is the symmetric velocity gradient (or strain rate) tensor. The kinematic viscosity ν is a simple function of the parameter ω. The constant k_2 and the link weights t_p are determined by the particular choice of lattice [7]. Note that, by using lattice isotropy properties, Eq. (5) may be inverted:

$$\mathbf{F}=k_2\sum_i\phi_i\mathbf{c}_i. \tag{8}$$

B. Multicomponent LB scheme

In order to adapt this method to model a multicomponent system, the momentum distribution function is specified in terms of the individual densities of the two immiscible fluids, designated red (R) and blue (B):

$$f_i(\mathbf{r},t)=R_i(\mathbf{r},t)+B_i(\mathbf{r},t), \tag{9}$$

with the nodal density of red and blue fluids defined as the separately conserved partial densities:

$$R(\mathbf{r},t)\equiv\sum_i R_i(\mathbf{r},t),\quad B(\mathbf{r},t)\equiv\sum_i B_i(\mathbf{r},t). \tag{10}$$

We note that Eqs. (3) and (4) remain valid for the *sum* fluid. Thus, even in an interfacial region the combined red and blue fluids define a fluid that evolves according to the LB evolution equation (2).

We define a phase field

$$\rho^N(\mathbf{r},t)\equiv\left(\frac{R(\mathbf{r},t)-B(\mathbf{r},t)}{R(\mathbf{r},t)+B(\mathbf{r},t)}\right), \tag{11}$$

where $-1\leq\rho^N(\mathbf{r})\leq 1$. Red and blue fluids mix in the LB propagation step; we define *mixed sites* as lattice sites that have both red and blue densities. The mixed sites form an interfacial region between the two fluids.

In order to induce a surface tension, it is possible to apply a force at the interface, $\mathbf{F}_{\rm st}(\mathbf{r})$, which is defined in terms of the gradient of $\rho^N(\mathbf{r})$ [8]. For an interface between two fluids of equal density, a cross-interfacial pressure step proportional only to the local curvature in the ρ^N field, H, results from the use of the fluid body force:

$$\mathbf{F}_{\rm st}(\mathbf{r})\equiv\frac{1}{2}\sigma H\nabla\rho^N, \tag{12}$$

where σ is the parameter controlling the strength of the surface tension. The negative of the normalized color gradient serves as the interface normal

$$\hat{\mathbf{n}}\equiv-\frac{\nabla\rho^N}{|\nabla\rho^N|}, \tag{13}$$

and the interface curvature H is obtained in two dimensions as the surface gradient,

$$H=n_xn_y\left(\frac{\partial n_x}{\partial y}+\frac{\partial n_y}{\partial x}\right)-n_x^2\frac{\partial n_y}{\partial y}-n_y^2\frac{\partial n_x}{\partial x}, \tag{14}$$

where there is no summation over repeated indices. Neglecting for simplicity the effects of spatial variation in the force $\mathbf{F}_{\rm st}$ [15,16], the required source term ϕ_i is obtained from Eq. (5).

C. Color segregation

The two fluids are segregated using the method of d'Ortona *et al.* [9] and Latva-Kokko and Rothman [10]. This is adopted because it is a simple and effective method for minimizing the presence of spurious velocities at the interface, a problem that besets many interface algorithms. In this method, the postcollision segregation of the two fluids is achieved using the algorithm

$$R_i = \frac{R}{R+B} f_i^{\dagger} + \beta \frac{RB}{R+B} t_p \cos(\theta_f - \theta_i) \mathbf{c}_i, \tag{15}$$

$$B_i = \frac{B}{R+B} f_i^{\dagger} - \beta \frac{RB}{R+B} t_p \cos(\theta_f - \theta_i) \mathbf{c}_i, \tag{16}$$

in which $(\theta_f - \theta_i)$ is the angle between the interface normal $\hat{\mathbf{n}}$ and the link direction. $f_i^{\dagger}$ denotes the postcollision value of the momentum density associated with link i. The segregation parameter $0 \leq \beta < 1$ controls the width of the interface and it is found empirically that a choice of $\beta \sim 0.7$ produces an interface which is as narrow as possible consistent with creating a very low level of spurious velocities.

III. LATTICE BOLTZMANN METHOD WITH DENSITY DIFFERENCE FORCE

The physical effects of a difference in density between two immiscible fluids, interacting at an interface, are captured by a fluid body force, the formulation of which we discuss first. We then proceed to consider its implementation. In this section we describe such a body force, then discuss its implementation with a multicomponent LB fluid algorithm.

A. Formulation

In this section we develop the means to simulate two mutually immiscible, incompressible fluids of very different densities, separated by a continuum interface.

We model this target system by considering the hydrodynamics equations that govern the flow of a *single* weakly compressible fluid and capture the behavior of the two immiscible fluids by the inclusion of gradients in density and viscosity close to the region of the interface between the two fluids.

The hydrodynamic equations describing the single fluid are the continuity equation

$$\frac{\partial \rho}{\partial t} + \frac{\partial (\rho v_\alpha)}{\partial x_\alpha} = 0, \tag{17}$$

and the Navier-Stokes equations for a compressible fluid [17]

$$\rho \left(\frac{\partial v_\alpha}{\partial t} + v_\beta \frac{\partial v_\alpha}{\partial x_\beta} \right) = - \frac{\partial p}{\partial x_\alpha} + \frac{\partial}{\partial x_\beta} \left[\eta \left(\frac{\partial v_\alpha}{\partial x_\beta} + \frac{\partial v_\beta}{\partial x_\alpha} - \frac{2}{3} \delta_{ij} \frac{\partial v_k}{\partial x_k} \right) \right] + \frac{\partial}{\partial x_\alpha} \left(\zeta \frac{\partial v_k}{\partial x_k} \right) + F_\alpha^{\text{ext}}, \tag{18}$$

where, in the last equation, ζ is the bulk viscosity, F_α^{ext} is an external force, and p is the pressure. The density of the fluid, ρ, we now write in the form

$$\rho = \varphi \rho_0, \tag{19}$$

where the quantity φ captures the change in density as one moves through the interface from one fluid to the adjacent fluid. φ is assumed to have significant spatial gradients only at the boundary between the two fluids and to be constant in the bulk of each fluid, with a value of either a (air) or w (water), where $a \leq \varphi \leq w$. Hence the density ρ takes a value between the density of the less dense (rare) component, $\rho_a = \rho_0$, and more dense component, $\rho_w = w\rho_0$. The variation in ρ_0 is assumed small. This assumption is found to be well justified in simulations, especially at large w values (see Fig. 2, below).

We consider a volume element advecting in the model fluid at the interface. Since the interface is stable, and the fluid is assumed to be essentially incompressible, the mass of this volume element is conserved. Consequently, the total material derivative of the density is zero everywhere in the model fluid:

$$\frac{\partial \rho}{\partial t} + v_\alpha \frac{\partial \rho}{\partial x_\alpha} = 0. \tag{20}$$

Therefore, from the continuity equation (17), it follows that

$$\frac{\partial v_\alpha}{\partial x_\alpha} = 0, \tag{21}$$

and the Navier-Stokes equation is now simplified:

$$\rho \left(\frac{\partial v_\alpha}{\partial t} + v_\beta \frac{\partial v_\alpha}{\partial x_\beta} \right) = - \frac{\partial p}{\partial x_\alpha} + \frac{\partial}{\partial x_\beta} \left[\eta \left(\frac{\partial v_\alpha}{\partial x_\beta} + \frac{\partial v_\beta}{\partial x_\alpha} \right) \right] + F_\alpha^{\text{ext}}. \tag{22}$$

Following the above arguments on the introduction of surface tension, we choose an external force

$$F_\alpha^{\text{ext}} = \frac{\sigma H}{\rho_a - \rho_w} \frac{\partial \rho}{\partial x_\alpha}, \tag{23}$$

which ensures that the cumulative forcing between the two components,

$$\int_a^w \frac{\sigma H}{\rho_w - \rho_a} \frac{\partial \rho}{\partial x_\alpha} dx_\alpha = \sigma H, \tag{24}$$

inserts Laplace law surface tension effects. The integral above is taken across the interface, between points corresponding to the bulk fluid components, σ is the surface tension coefficient, and H is a path-averaged interfacial curvature defined in Eq. (14). With this choice of interface force, the Navier-Stokes equation assumes an essentially incompressible form:

$$\rho \left(\frac{\partial v_\alpha}{\partial t} + v_\beta \frac{\partial v_\alpha}{\partial x_\beta} \right) = - \frac{\partial \delta p}{\partial x_\alpha} + \frac{\partial}{\partial x_\beta} \left[\eta \left(\frac{\partial v_\alpha}{\partial x_\beta} + \frac{\partial v_\beta}{\partial x_\alpha} \right) \right] + \frac{\sigma H}{\rho_w - \rho_a} \frac{\partial \rho}{\partial x_\alpha}. \tag{25}$$

We assume that flow velocities are everywhere small compared to the appropriate velocity of sound. Thus the sound velocity of each separated component (gas and liquid hereafter) is very large and further the sound velocities of the two components are approximately equal. We suppose an equation of state for our hypothetical fluid to be of the form

$$p = p_0 + c_s^2 \varphi(\rho_0 - \bar{\rho}_0), \tag{26}$$

where p_0 is a constant throughout the fluid and $\delta\rho_0 = (\rho_0 - \bar{\rho}_0)$ is the fluctuation in the density ρ_0 from the average density $\bar{\rho}_0$. We note that, at steady state and in the absence of a surface tension perturbation, $\delta\rho_0$ is zero. Accordingly, in this case, there would be no pressure drop across the interface. Proceeding, we further suppose that

$$\eta = \nu\rho = \nu\varphi\rho_0. \tag{27}$$

With substitutions from the last three equations, the Navier-Stokes equation (25) finally takes the form

$$\rho_0\left(\frac{\partial v_\alpha}{\partial t} + v_\beta \frac{\partial v_\alpha}{\partial x_\beta}\right) = -\frac{\partial}{\partial x_\alpha} c_s^2 \delta\rho_0 + \frac{\partial}{\partial x_\beta}(2\rho_0 \nu S_{\alpha\beta}) + F_\alpha. \tag{28}$$

Equation (28) is precisely the equation that is recovered using the LB algorithm, defined above for a lattice fluid of kinematic viscosity

$$\nu = \frac{1}{6}\left(\frac{2}{\omega} - 1\right)\frac{\delta x^2}{\delta_t}, \tag{29}$$

provided an effective force

$$F_\alpha = \bar{\sigma}_{\alpha\beta}\frac{\partial \ln \varphi}{\partial x_\beta} + \frac{\sigma H}{\rho_w - \rho_a}\frac{\partial \rho_0}{\partial x_\alpha} \tag{30}$$

is introduced. This force acts only at the interface and captures the static and dynamic effects of *both* the surfaces tension and the difference in density between the two fluids. In Eq. (30) we have defined

$$\bar{\sigma}_{\alpha\beta} = \left(-c_s^2 \delta\rho_0 + \frac{\rho_0}{\rho_w - \rho_a}\sigma H\right)\delta_{\alpha\beta} + \nu\rho_0\left(\frac{\partial v_\alpha}{\partial x_\beta} + \frac{\partial v_\beta}{\partial x_\alpha}\right). \tag{31}$$

Recall that the variation in ρ_0 is small relative to that in φ; consequently the second term in the right-hand side of Eq. (30) is negligible relative to the isotropic contribution to $\bar{\sigma}_{\alpha\beta}$ defined above.

Henceforth, we designate $\bar{\sigma}_{\alpha\beta}$ an *effective stress* tensor. In the right-hand side of Eq. (31), the isotropic component is responsible for hydrostatic inertial and interfacial tension effects at the interface. The term $2\nu\rho_0 S_{\alpha\beta}$ generates a shear-dependent force, again to adjust for inertia as the fluid density changes through the interface. Note that the densities of the separated components, ρ_a and ρ_w, are constants.

B. Implementation with the LB method

In order to extend the multicomponent LB interface method outlined in Sec. II to the case of separated components with different densities, we write our component density function φ in terms of the phase field ρ^N [see Eq. (11)] as follows:

$$\varphi = \frac{1}{2\rho_0}[(1+\rho^N)\rho_w + (1-\rho^N)\rho_a]. \tag{32}$$

Then the derivative of the logarithm of φ may be expressed through $\nabla\rho^N$, the color gradient:

$$\frac{\partial \ln \varphi}{\partial x_\beta} = \frac{\rho_w - \rho_a}{(\rho_w + \rho_a) + (\rho_w - \rho_a)\rho^N}\frac{\partial \rho^N}{\partial x_\beta} = \frac{\gamma - 1}{(\gamma + 1) + (\gamma - 1)\rho^N}\frac{\partial \rho^N}{\partial x_\beta}, \tag{33}$$

where the dimensionless density contrast parameter

$$\gamma = \frac{\rho_w}{\rho_a}. \tag{34}$$

Following the method of [8], Eqs. (33) and (31) are now used to define an appropriate macroscopic force; the corresponding source term $\phi_i(\mathbf{r})$ for the LBGK evolution equation (2) is, again neglecting spatial variation, obtained from Eq. (5).

C. Parametrization of LB implementation

When parametrizing our LB simulation method for a complex flow application, issues arise relating to the choice of (i) interfacial tension α and (ii) density contrast γ.

Let us consider the interfacial tension parameter α. Fluid in the immersed boundary, or interface, is described by Eq. (28). Using Eqs. (30) and (31) we approximate the external force term F_α in Eq. (28) with its dominant term to obtain

$$\frac{\partial v_\alpha}{\partial t} + v_\beta \frac{\partial v_\alpha}{\partial x_\beta} = -\frac{1}{\rho_0}\frac{\partial}{\partial x_\alpha} c_s^2 \delta\rho_0 + \frac{1}{\rho_0}\frac{\partial}{\partial x_\beta}(2\rho_0 \nu S_{\alpha\beta}) + \frac{\sigma H}{\rho_w - \rho_a}\frac{\partial}{\partial x_\alpha}\ln \varphi. \tag{35, 36}$$

Now, suppose for simplicity that the lattice density $\rho_0 = \rho_a$. Divide Eq. (35) by the fraction $\delta x/\delta_t^2$ and invoke the definition of lattice viscosity [Eq. (29)] to obtain the following description in which all velocities and distances are expressed in lattice units:

$$\frac{\partial v_\alpha^*}{\partial t^*} + v_\beta^* \frac{\partial v_\alpha^*}{\partial x_\beta^*} = -\frac{1}{\rho_0}\frac{\partial}{\partial x_\alpha^*} c_s^{*2} \delta\rho_0 + \frac{1}{\rho_0}\frac{\partial}{\partial x_\beta^*}(2\rho_0 \nu S_{\alpha\beta}^*) + \frac{\sigma^* H^*}{\rho_w - \rho_a}\frac{\partial}{\partial x_\alpha^*}\ln \varphi, \tag{37, 38}$$

where the physical interfacial tension σ and the lattice surface tension parameter σ^* are related by

$$\sigma^* = \sigma \frac{\delta_t^2}{\delta x^3}. \tag{39}$$

On eliminating the time step δ_t between Eqs. (39) and (29), we obtain for the lattice surface tension parameter

$$\sigma^* = \sigma \frac{\delta x (2/\omega - 1)^2}{36\nu^2}. \tag{40}$$

Clearly the parameter α^* controls the amplitude of the perturbative external force term $\phi_i(\mathbf{r})$ in lattice evolution equation (2); it must therefore be restricted in value. Accordingly, for target systems with large interfacial tension and small kinematic viscosity (large density) it is necessary to use small values of lattice spacing δx, which clearly increases computational cost, or values of $\omega \to 2$, which undermines stability.

Let us now consider the interfacial density contrast parameter γ. Take a point in the center of the interface, characterized by the phase field parameter $\rho^N = 0$. For this value of ρ^N, for given γ, the effective force *weight*, defined in Eq. (33), is a maximum. As γ increases, this weight increases (to its maximum value of unity) which increases the size of the effective force, undermining stability in regions where the strain rate is large [see the definition of effective stress in Eq. (31)]. Only by using small values of lattice spacing δx may the effective force contribution be regulated, with clear consequences for simulation efficiency.

In the application of our method to complex flow, in the next section, we consider a surface-breaching air bubble, diameter 1 cm, in water. The appropriate interfacial tension is very large and presents a challenge to our method. To simulate this system, we took

$$\nu = \nu_w \approx \nu_a = 10^{-6} \text{ m}^2 \text{ s}^{-1}, \quad \sigma \approx 7 \times 10^{-2} \text{ J m}^{-2}, \tag{41}$$

choosing to initialize the undeformed bubble to a radius of 1 cm, resolved on a fairly course mesh of 20 lattice units, so that $\delta x = 5 \times 10^{-4}$ m. This choice reflects the need to maintain a reasonable time step (see below).

As we have remarked, to limit the value of the lattice interfacial tension parameter σ^*, evaluated from Eq. (40), it was necessary to select a value of $\omega = 1.99$. The corresponding time step is then found to be $\delta_t = 2.1 \times 10^{-6}$ [from Eq. (29); note the quadratic dependence of δ_t on δx].

At our selected resolution, the shear rates developed at the cap edges of the breaching bubble (see Fig. 6) were observed to be large. In fact, it could be argued that this intense, local shear is itself a result of the shape assumed by the bubble and hence of the large interfacial tension—at smaller interfacial tension the local strains will relax as they deform the interface.

A key advantage of our method inherited from our original scheme, detailed in Sec. II B, is an ability to reach larger, controllable, interfacial tensions (consistent with smaller We and characteristic of many practical situations) which requires larger surface-tension-inducing forces or, equivalently, LB evolution equation source terms $\phi_i(\mathbf{r})$ in Eq. (2). This, in turn, increases the associated interfacial microcurrent. While Inamuro *et al.* [1] report a prohibitive increase in these spurious velocities for their multiphase LB simulations, for $\text{We} \geq 20$, we were able to achieve a $\text{We} \approx 3$ (evaluated from the bubble velocity just before it breaches the free surface) with small microcurrent activity, as the results of Figs. 6 and 7 demonstrate (Lee *et al.* and Mukherjee *et al.* achieve $\text{We} = 8000$ [2,6] and $\text{We} \geq 20$ in [1]).

From the considerations set out above, it was therefore necessary to restrict the density contrast, the data of Fig. 6 corresponding to $\gamma = 10$. This restriction may be easily overcome and larger density contrasts for this applications could be achieved with our method, most straightforwardly by increasing the spatial resolution (decreasing the values of δx and δ_t). However, it is important to note that, for a simulation of equivalent duration, the computational expense attending a twofold increase in simulation resolution is therefore 2^4. Furthermore, a density contrast of 10 is not particularly prohibitive in complex flow; the momentum transfer from the less dense fluid, once separated by an order of magnitude, may not be significantly altered by using a much larger density contrast.

D. Stabilization

The LB method is known to suffer instability in the form of local blowups and spurious oscillations when used to model high-Reynolds-number flow, or (as is the case here) with ω close to the limiting value of 2. In the application of our method to systems with realistic surface tensions, density differences, and drop Reynolds number, it was found necessary to stabilize the basic LB scheme, using the approach of Brownlee *et al.*[11].

The LB stabilization of Brownlee *et al.* is based upon thermodynamic considerations, adds no artificial dissipation, preserves the accuracy of the scheme and, not least, is algorithmically very simple to apply. By considering the LB evolution as a *free flight* (propagation) followed by a relaxation (collision) toward what is termed the *quasiequilibrium manifold* (of distribution functions f_i) Brownlee *et al.* have shown that the use of *coupled steps*, described below, considerably increases stability.

In practice, all that is necessary to implement the coupled-steps approach of Brownlee *et al.* to LB stabilization is to set the relaxation parameter $\omega = 1$ in Eq. (2), on alternate time steps, only on lattice nodes where a defined nonequilibrium entropy increases above a certain, fixed amount [11]. Clearly this is very simple to achieve. Using the extension of Brownlee *et al.*, the essential effect of which is to promote an evolution more closely adherent to the quasiequilibrium manifold (on which entropy is a maximum), our method achieved parametrizations typical of the real applications represented in Fig. 7.

IV. MODEL VALIDATION

The contribution of the term associated with $\delta_{\alpha\beta}$ in the effective stress tensor $\bar{\sigma}_{\alpha\beta}$ of Eq. (31) is apparent in static simulations. The static simulations represented in Figs. 1 and 2 relate to the steady state of an infinite array of circular drops of denser lattice fluid. The drops' initial radius was 16

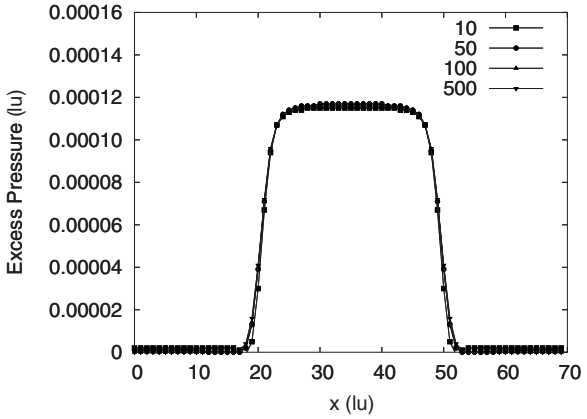

FIG. 1. Excess pressure profiles. Excess pressure δp_0 (measured in lattice units) is plotted with distance x (measured in lattice units) across a section of a static two-dimensional (2D) drop, initial radius 20 lattice units, for density contrasts $(\varphi_{\max}/\varphi_{\min})=10,50,100,500$. The corresponding density profiles are shown in Fig. 2.

lattice units and the data were obtained from a 70×70 lattice with periodic boundary conditions.

Note that, in both Figs. 1 and 2, the associated error bars are too small to resolve on the figures. The kinematic viscosity contrast between the rare and dense fluids is unity and the LB collision parameter $\omega=1$.

Figure 1 shows the variation of the excess pressure δp, computed from Eq. (26), with distance x along a continued diameter of equilibrated drops of initial radius 20 lattice units. The results are presented for a range of density contrast parameter $\gamma=5,10,50,100,500$ but with identical interfacial tension parameter α. The corresponding density variation is shown in Fig. 2. Note that, as the density contrast parameter γ increases, the lattice density ρ_0 shows reduced variation.

Figure 3 verifies Laplace law behavior. Note that this figure has a vertical axis which does not contain the origin. It

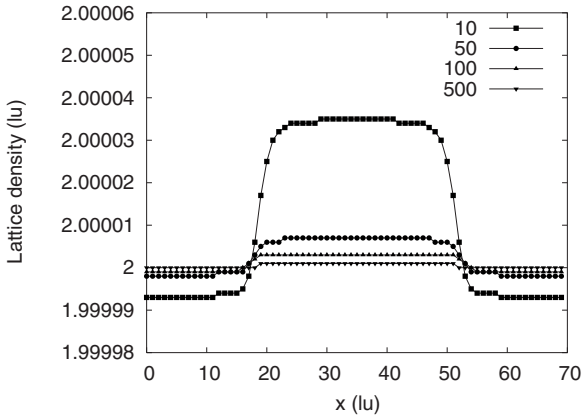

FIG. 2. Lattice density profiles (measured in lattice units) for an initial, uniform lattice density 2.0. Steady state lattice density ρ_0 is plotted with distance x (measured in lattice units) across a section of a static 2D drop, initial radius 20 lattice units, for density contrast parameter $(\varphi_{\max}/\varphi_{\min})=10,50,100,500$. The corresponding excess pressure profiles are shown in Fig. 1.

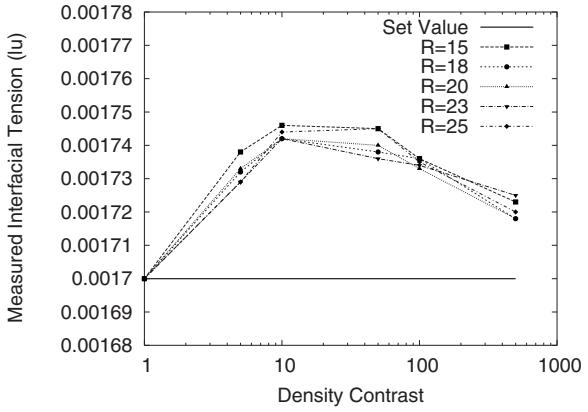

FIG. 3. Laplace law behavior. Pressure step (measured in lattice units), multiplied by initial drop radius (the effective interfacial tension), is plotted on the ordinate against density contrast parameter γ for the range of drop initial radii identified in the figure inset. The solid line indicates the set value of interfacial tension parameter α.

plots the measured pressure step, multiplied by drop radius (the effective interfacial tension), against the density contrast parameter γ for a range of initial drop radii R. The solid horizontal line indicates the set value of interfacial tension α. As $\gamma\to1$ we recover the expected behavior of our unmodified scheme [8]. The small increase ($<3\%$) observed in measured surface tension for intermediate values of γ we tentatively associate with the contribution to the interfacial force from outlying regions of the interface, characterized by $|\rho^N|\lesssim1$. The relative importance of this contribution diminishes as γ continues to increase [see Eq. (33), denominator].

The contribution of the term involving the velocity gradients in the effective tensor $\sigma_{\alpha\beta}$ of Eq. (31) is exposed only in dynamic simulations. Consider a planar rare/dense interface subject to a shear flow directed parallel to the interface. If the separated fluids have similar kinematic viscosity, the shear viscosity must change at the interface and the usual dynamic boundary conditions [17] therefore imply a change in the shear rate at the interface. In Figs. 4 and 5 the fluid interface occupies the region $28<y<32$: the rare and dense fluids occupy the regions $y>32$ and $y<28$, respectively.

Figure 4 shows the variation of the cross-interfacial phase field, the flow velocity, and the force component F_x parallel

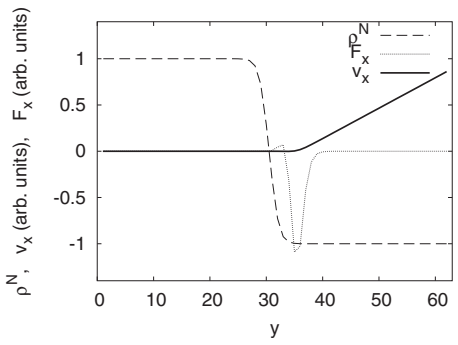

FIG. 4. Shear flow for density ratio (1000/1.3). Normalized cross-interfacial phase field ρ^N, force F_x, and velocity v_x, after Eq. (30), as a function of distance (measured in lattice units).

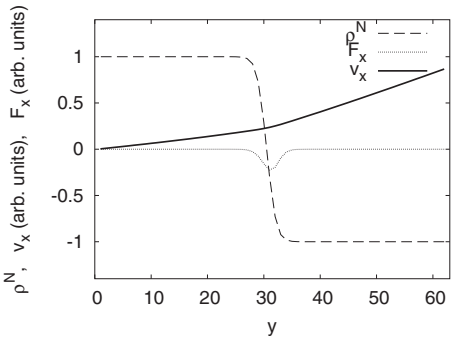

FIG. 5. Shear flow for density ratio 2. Normalized cross-interfacial phase field ρ^N, force F_x, and velocity v_x, after Eq. (30), as a function of distance (measured in lattice units).

to the flow velocity. These results are for fluids of large viscosity contrast and the quantities are plotted as functions of distance, measured perpendicular to the interface. Figure 5 shows similar data for an interface between fluids of smaller viscosity contrast. Comparing Figs. 4 and 5, we note that, for large density contrasts, the lighter fluid (on the right) is prevented from dragging along the *insulated*, heavier fluid (on the left).

Figure 6 shows phase field data at equal time intervals from a two-dimensional simulation of spatial resolution 450×450 lattice units, in which a bubble of less dense fluid rises under gravity and breaks the surface of the denser fluid. The surface tension is that between air and water and the initial radius of the droplet is 0.5 cm. Although the density contrast in this simulation is only 10, the correct gravitational forcing for air and water was used. The data of Fig. 6 show the formation, retraction, and collapse of an isolated cap under inertial, viscous, gravitational, and surface tension forces: its interpretation is discussed below. An initial release depth of the bubble, necessary to observe the formation of a jetlike structure (final three images), rather than satellite drops, was determined, by trial and error, to be 1.5 cm. Figure 7 shows the flow field associated with image 6 in Fig. 6. The maximum velocity vector near the core of the vortices has a value of approximately 0.145 m s^{-1}.

Consider the droplike features in Fig. 6 frames 12–15. It is known that surface instabilities cause water sheets in air to collapse into drops. Furthermore, Fig. 6 is in qualitative

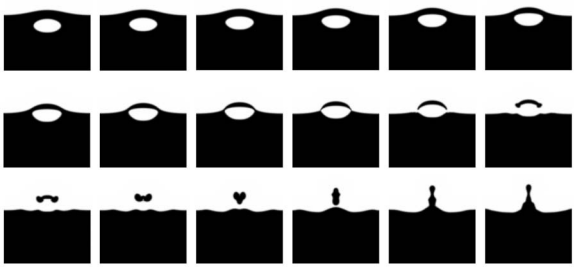

FIG. 6. Phase field, sampled at equal time intervals, from the simulation of an air bubble (white), initial diameter 1 cm, rising under gravity in water (black fluid). The initial bubble release depth was 1.5 cm.

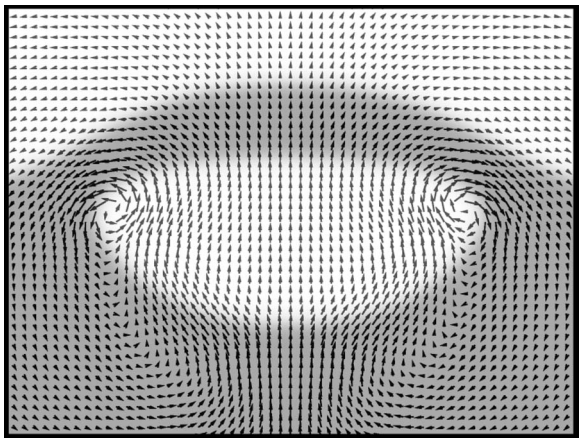

FIG. 7. Flow field associated with image 3 in Fig. 6.

agreement with the experimental data of Woodcock *et al.* [18], who obtained high-speed photographs of the fragments produced by bubbles of air, of a few millimeters diameter, bursting at an air-water interface. The results of Woodcock *et al.* show a jet of water projected vertically into the air and, in addition, some much smaller *satellite* droplets. However, the small drop structures (first evident in Fig. 6, frame 12), deriving from what is a two-dimensional simulation, must be interpreted with caution, as follows.

Close analysis of simulation flow and phase fields and the adequate resolution of the simulation (the drop structures in frame 12 have an approximate average radius of 18 lattice spacings) mean that the drop features, which form at the retracting cap tips, are not due to any numerical instability in our method. Noting that the system simulated in Figs. 6 and 7 has a central, vertical axis of symmetry, take the detaching cap tip in frame 12 of Fig. 6. There is positive interfacial curvature over the entire upper surface of this cap, which is, furthermore, large in the region of the cap tip. Beneath the cap, the surface curvature is positive only in the immediate tip region but it (surface curvature) rapidly becomes negative as one moves beneath the drop, toward the central axis of symmetry. Accordingly, in this two-dimensional simulation, interfacial tension forces tend strongly (i) to retract the drop tip locally, draining the cap fluid (water) into the nearby cap region, and (ii) to expand the underside of the cap—strongly close to the tip. These surface motions cause relatively rapid formation of drops in the cap tip region. Once formed, these drops cannot drain in the third dimension. It follows that drops formed at the retracting cap tip are topologically (but artificially) stabilized in our simulations.

While our method could easily be adapted to simulate a problem with axial symmetry (such as that in Fig. 6) with two-dimensional computational efficiency the collapse of the bubble cap, for this application, must be treated as a more resource-intensive, fully three-dimensional problem. However, such a detailed three-dimensional application of our method to the breaching bubble system would appear to be worth the expense.

V. CONCLUSION

We have presented a multicomponent LB simulation methodology designed for completely immiscible fluids with

large density contrast. Our method is stable over a large range of density contrasts, efficient, easy to implement, and, above all, local; it does not require, for example, an intermediate solution of the pressure field. The separated fluids' density difference is imposed on a relatively uniform LB fluid by introducing effective, shear-dependent forces acting only in the region of the interface; these forces compensate the relative fluid motion for inertial effects; see Figs. 4 and 5.

The paper presents a set of results from simulations implemented in two spatial dimensions which demonstrate the basic principles of the method and the recovery of the correct hydrostatic (see Figs. 1–3) as well as elementary hydrodynamic (see Figs. 4 and 5) behavior. We also present results corresponding to more complex multicomponent flow: these serve to demonstrate the utility of the method and its very real potential in continuum applications.

[1] T. Inamuro, T. Ogata, S. Tajima, and N. Konishi, J. Comput. Phys. **198**, 628 (2004).
[2] T. Lee and C. L. Lin, J. Comput. Phys. **206**, 16 (2005).
[3] A. J. Wagner and C. M. Pooley, e-print arXiv:cond-mat/0608480.
[4] H. W. Zheng, C. Shu, and Y. T. Chew, J. Comput. Phys. **218**, 353 (2006).
[5] N. Thurey, T. Pohl, U. Rude, M. Ochsner, and C. Korner, Comput. Fluids **35**, 934 (2006).
[6] S. Mukherjee and J. Abraham, Phys. Rev. E **75**, 026701 (2007).
[7] Y. H. Qian, D. d'Humieres, and P. Lallemand, Europhys. Lett. **17**, 479 (1992).
[8] S. V. Lishchuk, C. M. Care, and I. Halliday, Phys. Rev. E **67**, 036701 (2003).
[9] U. D'Ortona, D. Salin, M. Cieplak, R. B. Rybka, and J. R. Banavar, Phys. Rev. E **51**, 3718 (1995).
[10] M. Latva-Kokko and D. H. Rothman, Phys. Rev. E **71**, 056702 (2005).
[11] R. A. Brownlee, A. N. Gorban, and J. Levesley, Phys. Rev. E **74**, 037703 (2006).
[12] P. L. Bhatnagar, E. P. Gross, and M. Krook, Phys. Rev. **94**, 511 (1954).
[13] S. Succi, *The Lattice Boltzmann Equation for Fluid Mechanics and Beyond* (Clarendon, Oxford, 2001).
[14] S. Chapman and T. G. Cowling, *The Mathematical Theory of Non-Uniform Gases* (Cambridge University Press, Cambridge, U.K., 1995).
[15] Z. L. Guo, C. G. Zheng, and B. C. Shi, Phys. Rev. E **65**, 046308 (2002).
[16] I. Halliday, L. A. Hammond, C. M. Care, K. Good, and A. Stevens, Phys. Rev. E **64**, 011208 (2001).
[17] L. D. Landau and E. M. Lifshitz, *Fluid Mechanics* (Pergamon, Oxford, 1987).
[18] A. H. Woodcock, C. F. Kientzler, A. B. Arons, and D. C. Blanchard, Nature (London) **172**, 1144 (1953).